

Discovery of a redshift 6.13 quasar in the UKIRT Infrared Deep Sky Survey

D. J. Mortlock¹, M. Patel¹, S. J. Warren¹, B. P. Venemans², R. G. McMahon², P. C. Hewett², C. Simpson³, R. G. Sharp⁴, B. Burningham⁵, S. Dye⁶, S. Ellis⁷, E. A. Gonzales-Solares², and N. Huélamo⁸

¹ Astrophysics Group, Imperial College London, Blackett Laboratory, Prince Consort Road, London, SW7 2AZ, UK
e-mail: mortlock@ic.ac.uk

² Institute of Astronomy, University of Cambridge, Madingley Road, Cambridge, CB3 0HA, UK

³ Astrophysics Research Institute, Liverpool John Moores University, Twelve Quays House, Egerton Wharf, Birkenhead, CH41 1LD, UK

⁴ Anglo Australian Observatory, PO Box 296, Epping, NSW 1710, Australia

⁵ Centre for Astrophysics Research, Science and Technology Research Institute, University of Hertfordshire, Hatfield, AL10 9AB, UK

⁶ School of Physics & Astronomy, Queens Building, Cardiff University, The Parade, Cardiff CF24 3AA, UK

⁷ Institute of Astronomy, School of Physics, The University of Sydney, NSW 2006, Australia

⁸ Laboratorio de Astrofísica Espacial y Física Fundamental, European Space Astronomy Center, P.O. Box 78, E-28691 Villanueva de la Cañada, Madrid, Spain

Received 15 October 2008

ABSTRACT

Optical and near-infrared (NIR) spectra are presented for ULAS J131911.29+095051.4 (hereafter ULAS J1319+0950), a new redshift $z = 6.127 \pm 0.004$ quasar discovered in the Third Data Release (DR3) of the UKIRT Infrared Deep Sky Survey (UKIDSS). The source has $Y_{\text{Vega}} = 19.10 \pm 0.03$, corresponding to $M_{1450,\text{AB}} = -27.12$, which is comparable to the absolute magnitudes of the $z \approx 6$ quasars discovered in the Sloan Digital Sky Survey (SDSS). ULAS J1319+0950 was, in fact, registered by SDSS as a faint source with $z_{\text{AB}} = 20.13 \pm 0.12$, just below the signal-to-noise ratio limit of the SDSS high-redshift quasar survey. The faint z -band magnitude is a consequence of the weak Ly α /N v emission line, which has a rest-frame equivalent width of ~ 20 Å and provides only a small boost to the z -band flux. Nevertheless, there is no evidence of a significant new population of high-redshift quasars with weak emission lines from this UKIDSS-based search. The Ly α optical depth to ULAS J1319+0950 is consistent with that measured towards similarly distant SDSS quasars, implying that results from optical- and NIR-selected quasars may be combined in studies of cosmological reionization.

Also presented is a new NIR-spectrum of the previously discovered UKIDSS quasar ULAS J020332.38+001229.2, which reveals the object to be a broad absorption line quasar. The new spectrum shows that the emission line initially identified as Ly α is actually N v, leading to a revised redshift of $z = 5.72$, rather than $z = 5.86$ as previously estimated.

Key words. quasars: individual: ULAS J020332.38+001229.2; ULAS J131911.29+095051.4 – infrared: general – cosmology: observations

1. Introduction

Since their discovery by Schmidt (1963) and Hazard et al. (1963), quasars have continued to be the most revealing probes of the high-redshift Universe (e.g., Schneider 1999). Even though galaxies have been detected out to greater distances (e.g., IOK-1, with a redshift of $z = 6.96$, Iye et al. 2006) and gamma ray bursts may briefly be more luminous (e.g., Haislip et al. 2006), the highest-redshift quasars (e.g., SDSS 1148+5251 at $z = 6.42$, Fan et al. 2003; CFHQS J2329–0301 at $z = 6.43$, Willott et al. 2007) are more useful because they remain bright enough to be investigated in detail. It has been possible to obtain high signal-to-noise ratio (S/N) spectra for all the known $z \approx 6$ quasars, robustly confirming the nature of these sources, revealing their intrinsic properties (e.g., Walter et al. 2004; Venemans et al. 2007) and, through absorption, probing the intervening matter out to the quasars’ redshifts. The resultant measurements of the $z \approx 6$ quasar population are also of interest, as they provide critical limits on the early structure formation scenarios (e.g., Kurk et al. 2007). Probably the most dra-

matic discovery from these studies is the marked increase in the optical depth to neutral hydrogen at redshifts of $z \gtrsim 5.7$ (Becker et al. 2001; Fan et al. 2002, 2006a). The increase in optical depth appears to represent the end of cosmological reionization (e.g., Barkana & Loeb 2001), a conclusion supported by the *Wilkinson Microwave Anisotropy Probe* (WMAP; Bennett et al. 2003) measurements of the cosmic microwave background (e.g., Dunkley et al. 2009). While a consistent picture of reionization has emerged, the direct measurements of this process are limited to the small number of $z \approx 6$ quasars known, and it is clear that the discovery of quasars with $z \gtrsim 7$ is vital to further progress in this field.

The majority of the known $z \approx 6$ quasars have been identified by looking for point-sources with very red optical colours in wide-field surveys such as the Sloan Digital Sky Survey (SDSS; York et al. 2000) and the Canada France High- z Quasar Survey (CFHQS; Willott et al. 2007), and more discoveries will be made in such projects. Optical searches are, however, unlikely to probe beyond the current redshift limits. Almost all $z \approx 6$ quasar emis-

sion at rest-frame wavelengths shorter than the Ly α transition at $\lambda = 0.1216\mu\text{m}$ is absorbed by intervening hydrogen, and such quasars are effectively dark at observed wavelengths below $\lambda \approx [0.85 + 0.12(z - 6)]\mu\text{m}$. Conversely, most optical charge-coupled device (CCD) detectors have a poor response beyond wavelengths of $\lambda \approx 1\mu\text{m}$ (i.e., redward of the z or Z bands), so quasars with a redshift of $z \gtrsim 6.4$ are destined to remain invisible to CCD-based surveys. Given the rarity of $z \gtrsim 6$ quasars (e.g., a surface density of $\sim 0.02\deg^{-2}$ to $z_{\text{AB}} = 21.0$; Jiang et al. 2007), progress can only be made using wide-field surveys at longer wavelengths.

In the long term, radio surveys with, e.g., the Low Frequency Array (LOFAR¹) and the Square Kilometre Array (SKA²) will provide a powerful complementary approach (e.g., Wyithe et al. 2009), but the first steps beyond the current limits will come in the near-infrared (NIR), with surveys following the same basic principles as the SDSS and CFHQS searches. The largest completed NIR survey, the Two Micron All Sky Survey (2MASS; Skrutskie et al. 2006), with a magnitude limit of $J_{\text{Vega}} \approx 15.8$, does not have sufficient depth to find any plausible high-redshift quasars. The Visible and Infrared Survey Telescope for Astronomy (VISTA; Emerson et al. 2004) should cover $\sim 2 \times 10^4\deg^2$ to $J_{\text{Vega}} \approx 20$ during the next decade, but progress in the search for high-redshift quasars will come first from the partially complete UKIRT Infrared Deep Sky Survey (UKIDSS; Lawrence et al. 2007).

One new high-redshift quasar, ULAS J020332.38+001229.2, hereafter ULAS J0203+0012, with an estimated redshift of $z = 5.86$ (Venemans et al. 2007), has already been discovered in UKIDSS; the second such discovery, ULAS J131911.29+095051.4, hereafter ULAS J1319+0950, is presented here. Section 2 gives an introduction to the UKIDSS LAS project and Section 3 describes the selection techniques that led to ULAS J1319+0950 being identified as a candidate high-redshift quasar. Optical and NIR spectra of ULAS J1319+0950 are presented and compared to those of $z \approx 6$ SDSS quasars in Section 4. In addition, a new NIR spectrum of ULAS J0203+0012 is presented in Section 5, together with a revised redshift estimate for this source. The conclusions and future prospects for high-redshift quasar searches with UKIDSS are discussed in Section 6.

All photometry is given in the native system of the telescope in question, and explicitly subscripted. Thus SDSS i and z photometry is on the AB system, whereas UKIDSS Y and J photometry is Vega-based. The AB corrections for the UKIDSS bands are $Y_{\text{AB}} = Y_{\text{Vega}} + 0.634$ and $J_{\text{AB}} = J_{\text{Vega}} + 0.938$ (Hewett et al. 2006). Calculations of absolute (AB) magnitudes are performed assuming a fiducial flat cosmological model with normalised matter density $\Omega_m = 0.27$, normalised vacuum density $\Omega_\Lambda = 0.73$, and Hubble constant $H_0 = 71\,\text{km}\,\text{s}^{-1}\,\text{Mpc}^{-1}$.

2. The UKIRT Infrared Deep Sky Survey

UKIDSS (Lawrence et al. 2007) is a suite of five surveys undertaken with the Wide Field Camera (WFCAM; Casali et al. 2007) on the 3.8 m United Kingdom Infrared Telescope (UKIRT) at Mauna Kea, Hawaii. The WFCAM detectors are four sparse-packed 2048×2048 Rockwell Hawaii-II arrays, each of which has a field of view of $0.05\deg^2$. Observations are generally undertaken in sets of four contiguous pointings which, together, cover $0.77\deg^2$. Full details of the survey operations can be

found in Dye et al. (2006). The individual images are analysed by the data reduction pipeline described by Irwin et al. (2009) and the catalogues of detected objects are merged across bands into a queryable relational database at the WFCAM Science Archive³ (WSA; Hambly et al. 2008).

The UKIDSS Large Area Survey (LAS) will cover $4000\deg^2$ within the SDSS footprint with a series of 40 s exposures⁴ in the Y , J , H and K bands. The resulting magnitude limits are typically $Y_{\text{Vega}} \approx 20.2$, $J_{\text{Vega}} \approx 19.6$, $H_{\text{Vega}} \approx 18.8$ and $K_{\text{Vega}} \approx 18.2$ for point-sources detected with $S/N \approx 5$, and the average seeing is $0''.8$ (Warren et al. 2007). The area, depth and wavelength coverage of the LAS were chosen with the detection of $z \approx 6$ quasars in mind, and the Y filter, positioned between the z and J bands in a region of minimal atmospheric absorption ($0.97\mu\text{m} \lesssim \lambda \lesssim 1.07\mu\text{m}$), is particularly useful in this regard (Hewett et al. 2006). Quasars in the redshift interval $6.4 \lesssim z \lesssim 7.2$ would be identifiable as being unusually red in $i-Y$ and $z-Y$, while being significantly bluer in $Y-J$ than the more numerous L and T dwarfs.

All UKIDSS images and catalogues are made available to European Southern Observatory (ESO) countries and then, 18 months later, the world, in a series of incremental data releases. The results presented here are based on the Third Data Release (DR3; Warren et al. 2009) for which there is $870\deg^2$ of LAS coverage in the Y and J bands.

3. Candidate selection

High-redshift quasar candidates are selected in a two-step process, using survey data initially (Section 3.1), followed by additional photometric observations of the most promising objects (Section 3.2).

3.1. Initial shortlist

Redshift ~ 6 quasars are expected to appear as stationary point-sources with extremely red optical–NIR colours. The first stage of the candidate selection process is to extract a fairly complete (if highly contaminated) sample of all such sources from the UKIDSS and SDSS databases.

The initial selection from the UKIDSS LAS was of all point-sources with $Y_{\text{Vega}} \leq 19.88$ that were also detected in the J band and have measured $Y_{\text{Vega}} - J_{\text{Vega}} \leq 0.88$ (to exclude L and T dwarfs). The resulting sample was then cross-matched to the SDSS Fifth Data Release (DR5; Adelman-McCarthy et al. 2007) and all sources either undetected by SDSS or with $i_{\text{AB}} - Y_{\text{Vega}} \geq 2.5$ (but undetected in u , g and r) were selected. Any sources with inter-band (or inter-survey) positional mis-matches of greater than $0''.7$ were rejected to avoid nearby Galactic stars with appreciable proper motions, as well as most asteroids⁵.

A number of heuristic algorithms were applied to reject sources for which the UKIDSS or SDSS database photometry is likely to be unreliable. Contaminating sources eliminated at this stage include those arising from WFCAM cross-talk (Dye et al. 2006), objects in the haloes of bright stars, and close pairs separated by a few arcsec for which deblending is required in SDSS.

³ The WSA is located at <http://surveys.roe.ac.uk/wsa/>.

⁴ 80 s exposures are sometimes taken in mediocre conditions, an example of which is the finding chart shown in Fig. 1.

⁵ Some asteroids, observed at a turning point between prograde and retrograde motion, can appear stationary in UKIDSS survey images taken within an hour of each other.

¹ See the LOFAR web-site at <http://www.lofar.org/>.

² See the SKA web-site at <http://www.skatelescope.org/>.

For the sources that were undetected in SDSS i and z , aperture fluxes, corrected for aperture loss, were measured from the SDSS images. Acquisition of the aperture fluxes represents the final step in a fully automatic procedure that, in the analysis of UKIDSS DR3, yielded $\sim 2 \times 10^4$ pre-candidates with i -, z -, Y - and J -band photometry.

The next stage of the selection process is to use Bayesian model comparison to determine the probability, given the photometric data, that each source is a high-redshift quasar, P_q . This calculation is described in detail in Mortlock et al. (2009). The key to this approach is having an accurate model of the stellar population, specifically the intrinsic magnitude and colour distributions of the cool M dwarfs which scatter into the quasar selection box described above. Convolving this distribution in i , z , Y and J with the observational noise gives the likelihood that any candidate is an M dwarf. This can be compared directly with the likelihood that the candidate is a quasar, which is calculated using an extrapolation of the high-redshift quasar luminosity function of Fan et al. (2004) and simulated colours from Hewett et al. (2006). The result is a fully self-consistent value of P_q that, in principle, combines the available information on the candidate with the constraints on the quasar and star populations in an optimal way. Of course there are practical limitations, the most important of which result from incomplete sampling of the tails of the noise distributions and the limited knowledge of the stellar population fainter than the UKIDSS and SDSS survey limits. The latter is important as the probability calculation necessarily includes the possibility of faint sources scattered into the sample, but is difficult to assess empirically using the survey data. Despite these ambiguities (which are explored further in Mortlock et al. 2009), the probabilities which result from the adopted noise and population models clearly provide a good objective ranking scheme for quasar candidates.

Most of the candidates are clustered close to the stellar locus and their low quasar probabilities (i.e., $P_q \lesssim 0.01$) merely confirm the obvious. The motivation for the method is to assess the ambiguous sources lying between the quasar and star loci in colour space, or close to the Y -band limit with quasar-like colours but large errors. The sometimes counter-intuitive results are explored in some detail in Mortlock et al. (2009), but the critical point is that the candidates can be ranked by P_q and thus prioritised objectively for further investigation.

It is only at this stage that any visual inspection was undertaken, with the UKIDSS and SDSS images of the few hundred best candidates checked for artefacts such as hot pixels, bad columns, obviously wrong photometry, and undetected, blended or moving sources. (Although the UKIDSS and SDSS data reduction pipelines flag the vast majority of such instances, the selection of unusual sources on the basis of observed inter-survey colours inevitably produces samples with an over-representation of the very rare cases for which at least one of the surveys has produced anomalous measurements.) Following visual inspection, only a small sample of $\lesssim 100$ plausible quasar candidates with $P_q \gtrsim 0.01$ remained⁶, one of which was ULAS J1319+0950, shown in Fig. 1. Follow-up observations were needed to either reject these candidates as stars or, hopefully, confirm some as high-redshift quasars.

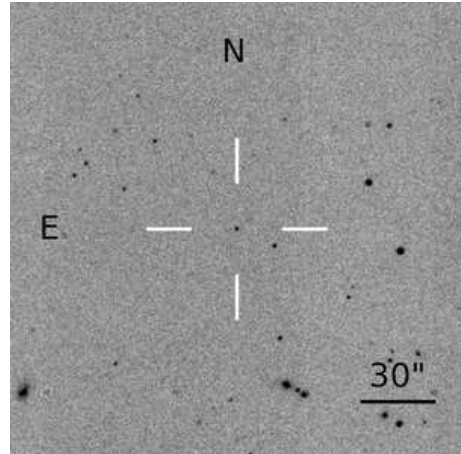


Fig. 1. Finding chart for ULAS J131911.29+095051.4 showing the UKIDSS LAS 80 s J -band image of a field 3 arcmin on a side centred on the source position at RA = 199.79706 deg and dec = 9.84762 deg.

3.2. Follow-up photometry

Rather than immediately taking spectra of all the candidates (cf Glikman et al. 2008), it is more efficient first to refine the photometry, obtaining short exposures in the i , z , Y and J bands on a variety of telescopes. The quasar probability defined in Section 3.1 is recalculated whenever new data are obtained, and a source is dropped from the candidate list if P_q falls below the selection threshold at any point. As almost all the candidates initially have minimal S/N in the i band SDSS images, follow-up observations in this band are the most efficient way to quickly reject such sources, revealing most to be cool stars scattered to have quasar-like colour by photometric noise. Observations in i are thus prioritised, although initial follow-up observations are sometimes made in z , Y or J , depending on weather, telescope scheduling, and other external factors. Candidates are not considered for spectroscopy until follow-up photometry has been obtained in at least the i , Y and J bands.

Follow-up observations of ULAS J1319+0950 were obtained in i , z , Y and J , as summarised in Table 1.

ULAS J1319+0950 was first re-observed in the i band at the Liverpool Telescope (LT) on the nights beginning 2008 January 8 and 12 for a total of 3240 s. The candidate's quasar probability remained high, and so 300 s exposures in each of the Y and J bands were obtained using the UKIRT Fast-Track Imager (UFTI) on the night beginning 2008 January 16. The candidate still appeared promising so the UFTI observations were repeated the following night.

The improved i -, Y - and J -band measurements were sufficiently precise that ULAS J1319+0950 had $P_q \simeq 1$ (i.e., it was essentially implausible for a cool star to have scattered to the candidate's observed colours given the precision of the new photometric data), whereas all the other initial candidates were rejected on the basis of their follow-up photometry. A spectrum of ULAS J1319+0950 was thus obtained on the night beginning 2008 January 22, with the result that it was immediately confirmed as a high-redshift quasar (Section 4). That the entire selection, follow-up and confirmation process for ULAS J1319+0950 was completed less than seven weeks after the UKIDSS DR3 release (on 2007 December 6) is a powerful illustration of the advantages of queue-scheduling for the three

⁶ The choice of threshold value for P_q (which defines the list of candidates and determines the completeness and contamination of the quasar sample) depends on the resources available for follow-up photometry and spectroscopy.

telescopes involved, especially considering the RA of the target and the time of year.

ULAS J1319+0950 had already been detected as a faint source in SDSS, although with $z_{AB} = 20.13 \pm 0.12$ its S/N was too low for it to be selected into the high-redshift quasar sample defined by Fan et al. (2003). Post-confirmation, improved z -band photometry of ULAS J1319+0950 was obtained using the ESO Multi-Mode Instrument (EMMI) on the New Technology Telescope (NTT) on the night of 2008 January 29. The observations were made with the long-pass #611 filter, the bandpass of which, in combination with the red cut-off of the CCD response, is quite similar to the SDSS z bandpass (Venemans et al. 2007). To calibrate the NTT-image, SDSS i - and z -band photometry of bright, unsaturated stars in the frame was converted to the natural system of the image using $z_{\text{NTT,AB}} = z_{AB} - 0.05(i_{AB} - z_{AB})$ (Venemans et al. 2007), and the result quoted in Table 1 is in this natural system.

4. ULAS J1319+0950

After the series of follow-up photometric observations described in Section 3.2 showed ULAS J1319+0950 to be a promising high-redshift quasar candidate, an optical spectrum was obtained to confirm the identification (Section 4.1). A more accurate redshift was estimated from a NIR spectrum covering the Mg II emission line (Section 4.2), after which both spectra were used to compare ULAS J1319+0950's emission and absorption properties with those of similarly distant quasars discovered in SDSS (Section 4.3).

4.1. Spectroscopic observations

An optical spectrum of ULAS J1319+0950 was obtained using the Gemini Multi-Object Spectrograph (GMOS) on the Gemini South Telescope on the night beginning 2008 January 22. Two spatially-offset spectra, each of duration 900 s, were obtained using a $1''.0$ slit and the R400 grating, covering the wavelength range of 0.5 – $1.0 \mu\text{m}$ over the three CCDs. The standard bias subtraction and flat-fielding steps were followed. Then, because of the strong sky lines in the red part of the spectrum, the ‘double subtraction’ method was used for the first-order sky subtraction (i.e., frame B was subtracted from frame A, and then the negative spectrum subtracted from the positive spectrum, after the two spectra were aligned). This procedure removes most systematic errors, but at the price of increasing the noise in the final frame by a factor of ~ 1.4 compared to the theoretical limit. Second-order sky subtraction was achieved by fitting a smooth function to each column. At this point cosmic rays were removed using the Laplacian Cosmic Ray Removal Algorithm (LCRRA; van Dokkum 2001). Wavelength-calibration was carried out using observations of a Cu Ar lamp. Relative spectrophotometry, and correction for telluric absorption, was achieved using observations of a standard star, and the spectrum was then scaled to match the NTT z -band photometry given in Table 1. The final GMOS spectrum is shown in Fig. 2.

The spectrum is recognisable as that of a $z \simeq 6$ quasar from the presence of a broad emission line, identified as Ly α , at the same wavelength as a strong continuum break, attributed to Ly α forest absorption. The Ly α emission peaks at a wavelength of $\lambda \simeq 0.88 \mu\text{m}$, which leads to a preliminary redshift estimate of $z = 6.12$. However the Ly α line is strongly absorbed to the blue and such high-ionization lines can exhibit velocity shifts relative to the quasar systemic redshift (e.g., Tytler & Fan 1992), limiting the utility of the optical redshift measurement.

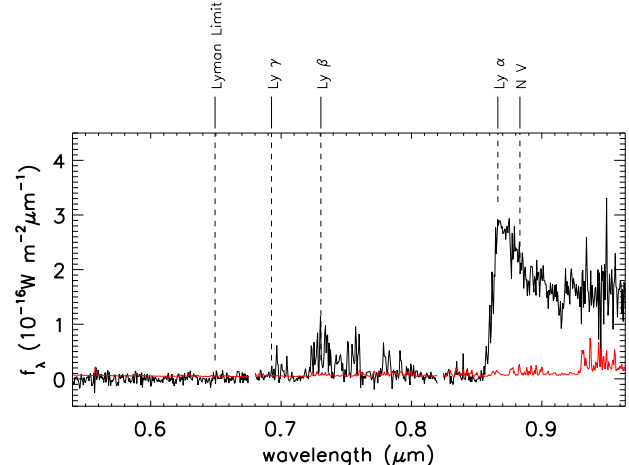


Fig. 2. The Gemini GMOS spectrum of ULAS J1319+0950 (black curve) and the noise spectrum (red curve), both binned by a factor of four. The gaps at wavelengths of $\sim 0.68 \mu\text{m}$ and $\sim 0.82 \mu\text{m}$ correspond to the breaks between the different CCDs. The wavelengths of common emission lines redshifted by $z = 6.13$ are indicated.

The Mg II line, if observable in the K band, should give a more reliable estimate of the redshift, and so a NIR spectrum of ULAS J1319+0950 was obtained. The source was observed using the Near-IR Instrument (NIRI) on the Gemini North Telescope on the two nights beginning 2008 February 26 and 27. Observations were made with a $0''.75$ slit and the K grism G5204, covering the wavelength range 1.9 – $2.5 \mu\text{m}$ with a resolving power of $R = 500$. With NIRI it is standard procedure to discard the first exposure of a sequence, leaving a total of 11 usable 300 s exposures over the two nights. The observation and data reduction methodology of Weatherley et al. (2005) was adopted, with six different slit positions used to reduce the noise from sky-subtraction relative to the more standard ABBA sequence. The data suffered from increasing slit losses as the observations proceeded, which is believed to be due to differential flexure between the guide probe and the instrument. The additional slit losses, relative to the first frames on each night, reduced the final S/N of the detected emission line by a factor of ~ 1.5 . Because of the varying throughput, each sky-subtracted frame was first scaled to a common count level, and then weighted by the inverse variance in the sky (as evaluated in a region free of strong emission lines). Wavelength calibration was performed using the list of sky emission lines from Rousselot et al. (2000). A standard star observed at similar airmass was used to correct for telluric absorption, and for relative flux calibration, after which the spectrum was scaled to match the UKIDSS K -band photometry given in Table 1. The final NIR spectrum is plotted in Fig. 3.

4.2. Redshift estimation

The NIR spectrum of ULAS J1319+0950 shown in Fig. 3 reveals the broad Mg II emission line near $\lambda \simeq 2.0 \mu\text{m}$, corroborating the initial redshift estimate of $z \simeq 6.1$. To obtain a more accurate measurement (and to quantify the absorption in the Ly α forest in Section 4.3) a power-law fit to the continuum was made to the combined optical and NIR spectrum by minimizing χ^2 and iteratively clipping outliers to eliminate the emission lines. The best-fit power-law is $f_\lambda(\lambda) \propto \lambda^{-(2-\alpha)}$, where $\alpha = 0.32 \pm 0.01$ (defined so that $f_\nu \propto \nu^{-\alpha}$). This is plotted in Fig. 4. This continuum was subtracted from the data and then a Gaussian was fit to the

Table 1. Original survey and follow-up photometric observations of ULAS J1319+0950.

filter	original	follow-up	observing date	telescope	exposure time
i_{AB}	22.83 ± 0.32	22.55 ± 0.09	2008 January 8 and 12	LT	2×1620 s
z_{AB}	20.13 ± 0.12	19.99 ± 0.03	2008 January 29	NTT	450 s
Y_{Vega}	19.22 ± 0.06	19.10 ± 0.03	2008 January 16 and 17	UKIRT	2×300 s
J_{Vega}	18.69 ± 0.05	18.76 ± 0.03	2008 January 16 and 17	UKIRT	2×300 s

All magnitudes are quoted in the natural system of the initial survey: AB for the optical SDSS bands and Vega for the NIR UKIDSS bands. Note that the transmission profile of the z_{NTT} filter differs somewhat from that of the SDSS z filter (see Section 3.2).

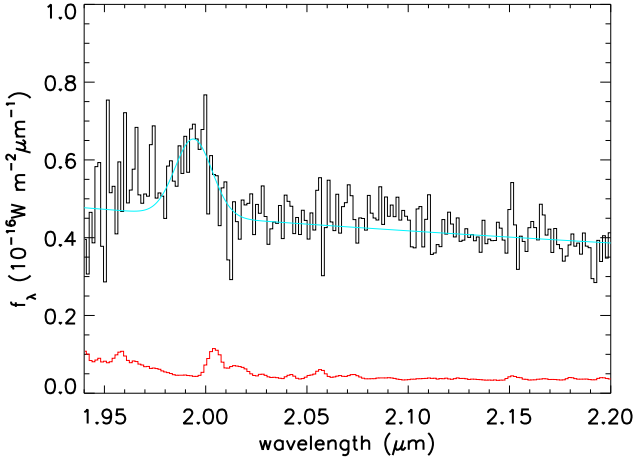


Fig. 3. The Gemini NIRI spectrum of ULAS J1319+0950 (black curve) and the error spectrum (red curve), both binned by a factor of two. The continuum+line fit to the Mg II emission line is also shown (blue). The fit implies a source redshift of $z = 6.127 \pm 0.004$. The effect of telluric absorption was removed using a standard star observed at similar airmass, resulting in the increased errors at $\sim 2.005 \mu\text{m}$.

residual Mg II emission line; the resultant continuum+line fit is plotted in Fig. 3. The central wavelength of the Mg II emission is $\lambda = (1.994 \pm 0.001) \mu\text{m}$, implying that ULAS J1319+0950 has a redshift of $z = 6.127 \pm 0.004$. The Mg II emission line has a rest-frame equivalent width of $\sim 14 \text{ \AA}$, substantially less than the typical value of $\sim 28 \text{ \AA}$ for $z \approx 6$ quasars found by Kurk et al. (2007).

4.3. Comparison with SDSS quasars

ULAS J1319+0950 is, after ULAS J0203+0012 (Venemans et al. 2007), only the second redshift ~ 6 quasar discovered in the NIR. Given that surveys at these wavelengths are the first capable of probing beyond the current limit of $z \approx 6.4$, it is important to determine whether quasars selected in the NIR exhibit significant differences from those selected in the optical. This preliminary exploration focuses on the emission line strengths, the neutral hydrogen optical depth, and the ionization region around the quasar.

4.3.1. Emission line properties

Redshift ~ 6 quasars are identifiable in photometric surveys primarily due to their extreme colours which result from the strong neutral hydrogen absorption blueward of the quasars' Ly α emission lines. However Fig. 5, which compares the rest-frame spectrum of ULAS J1319+0950 (and ULAS J0203+0012;

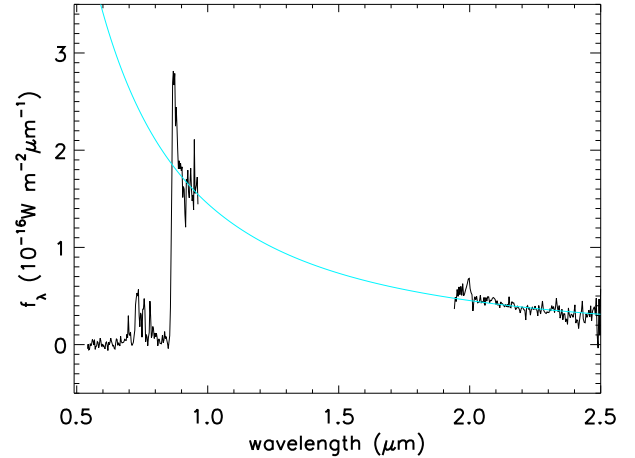


Fig. 4. The optical spectrum, binned by a factor of four (left black curve), and the NIR spectrum, binned by a factor of five (right black curve), of ULAS J1319+0950. The power-law continuum fit is also shown (blue).

see Section 5) to a composite SDSS quasar spectrum (Fan et al. 2006b), shows that ULAS J1319+0950 has a noticeably weaker Ly α emission line than is typical for optically-identified sources.

Measuring the rest-frame equivalent width of ULAS J1319+0950's Ly α line is somewhat problematic as the continuum level is ambiguous and the power-law fit shown in Fig. 4 is probably too steep to give a good local continuum estimate. For the purposes of comparison the continuum levels shown in Fig. 5 were adopted, yielding rest-frame equivalent widths of 19.3 \AA for ULAS J1319+0950 and 60.2 \AA for the Fan et al. (2004) composite. This quantifies the visual impression that ULAS J1319+0950 has a weaker Ly α emission line than an average $z \approx 6$ quasar, although there are several examples of high-redshift quasars with even weaker lines (e.g., Fan et al. 1999; Diamond-Stanic et al. 2009).

If ULAS J1319+0950 differed only in that its Ly α emission was marginally stronger (or, equivalently, less absorbed to the blue), it would almost certainly have been discovered in the SDSS high-redshift quasar sample. With $z_{\text{AB}} = 20.13 \pm 0.12$ in the SDSS database, it was brighter than the Fan et al. (2003) limit of $z_{\text{AB}} = 20.2$, but it failed the S/N cut of $\sigma_{z_{\text{AB}}} < 0.1$. Given that the NTT re-observation described in Section 3.2 gave $z_{\text{AB}} = 19.99 \pm 0.03$, the SDSS team were unlucky that the measured z -band flux was less than the true value and that the source was observed in slightly worse than average conditions, both of which combined to leave the source outside their selection cuts. This illustrates the more general limitation inherent in any selection method which applies a hard data cut in a region of parameter space where there are appreciable numbers of objects. A way to avoid the problem, at least in principle, is to apply the proba-

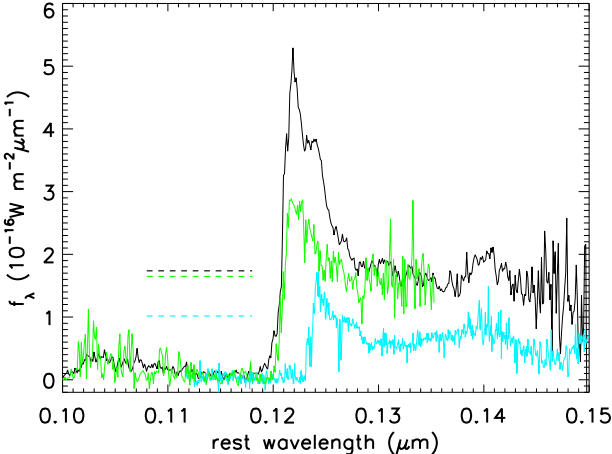


Fig. 5. Rest-frame spectra of ULAS J0203+0012 (blue) and ULAS J1319+0950 (green) compared to the composite spectrum of $z \approx 6$ SDSS quasars presented by Fan et al. (2004). The continuum level adopted for the calculation of the equivalent width of the Ly α line for each spectrum is also shown (dashed lines).

bilistic approach adopted in Section 3.1 and described in full by Mortlock et al. (2009), although it remains difficult to deal with the large numbers of low S/N candidates near the survey limit.

4.3.2. Neutral hydrogen optical depth

Observations of $z \approx 6$ quasars have revealed a marked increase in the density of neutral hydrogen above a redshift of ~ 5.7 (e.g., Fan et al. 2002), possibly indicating the end of cosmological reionization (e.g., Fan et al. 2006a). As hydrogen absorption also has an effect on the detectability of $z \approx 6$ quasars, it is important to assess whether the measured optical depths of optical- and NIR-selected quasars differ significantly.

Here, the spectrum of ULAS J1319+0950 is analysed following the method of Fan et al. (2006a), with the effective optical depth, $\tau_{\text{eff}}(z_{\text{abs}})$, at redshift z_{abs} estimated to be

$$\tau_{\text{eff}}(z_{\text{abs}}) = -\ln \left\{ \frac{\langle f_{\lambda,\text{obs}}[(1+z)\lambda_{\text{Ly}\alpha}] \rangle_{z=z_{\text{abs}}}}{\langle f_{\lambda,\text{int}}[(1+z)\lambda_{\text{Ly}\alpha}] \rangle_{z=z_{\text{abs}}}} \right\}, \quad (1)$$

where $f_{\lambda,\text{obs}}(\lambda)$ is the observed flux density, $f_{\lambda,\text{int}}(\lambda)$ is the continuum flux density (assumed to be given by the power-law fit described in Section 4.2), and $\lambda_{\text{Ly}\alpha} = 0.1216 \mu\text{m}$ is the rest-frame wavelength of the Ly α transition. The angle brackets denote an averaging over a finite redshift range around z_{abs} ; bins of width $\Delta z_{\text{abs}} = 0.15$ were used. Given that the Ly β and Ly α emission lines appear at $\lambda = 0.74 \mu\text{m}$ and $\lambda = 0.87 \mu\text{m}$, respectively, $\tau_{\text{eff}}(z_{\text{abs}})$ can be estimated in the range $5.1 \lesssim z_{\text{abs}} \lesssim 6.0$. The errors in these optical depth estimates are dominated by the noise in the spectrum of ULAS J1319+0950, with the uncertainties in the continuum fit and sample variance (across different lines-of-sight) being secondary. The resultant error bars are also significantly asymmetric, especially for the $z_{\text{abs}} = 5.93$ bin, in which flux is detected with only $S/N \approx 2$. These Ly α optical depth estimates, along with an analogous estimate of the Ly β optical depth (with the Ly α emission corrected for as described by Fan et al. 2006a), are given in Table 2.

These estimated optical depths towards ULAS J1319+0950 are consistent with measurements of SDSS quasars by Fan et al. (2006a), which gives some confidence that Gunn & Peterson (1965) effect measurements of optical- and NIR-selected $z \approx 6$ quasars may be combined.

Table 2. Effective optical depths of the absorption systems seen in the spectrum of ULAS J1319+0950.

transition	z_{abs}	τ_{eff}
Ly α	5.93	$3.59^{+0.71}_{-0.41}$
Ly α	5.78	$4.27^{+0.45}_{-0.31}$
Ly α	5.63	$3.35^{+0.13}_{-0.11}$
Ly α	5.48	$2.58^{+0.12}_{-0.12}$
Ly α	5.33	$3.21^{+0.15}_{-0.13}$
Ly α	5.18	$1.94^{+0.03}_{-0.03}$
Ly β	5.88	$2.43^{+0.06}_{-0.06}$

The Ly β optical depth has been corrected for Ly α absorption using the relation found by Fan et al. (2006a).

4.4. Quasar ionization region

The ultraviolet (UV) photons from quasars are sufficiently energetic to ionize the neutral hydrogen in a volume around them, creating a Strömgren (1939) sphere. The extent of the ionization region depends in part on the UV luminosity of the quasar and the neutral fraction of the surrounding medium, potentially providing a complementary probe of reionization. Unfortunately, the measurement is difficult in practice, due to uncertainties in the quasars' UV spectral energy distributions (SEDs), unknown ionizing flux from nearby galaxies, and difficulty in establishing the extent of the H II region from heavily absorbed and otherwise noisy spectra (e.g., Fan et al. 2006a).

It has proved more useful to adopt a relative approach in which the evolution of the size of quasars' H II regions with redshift is estimated without reference to an absolute model of the neutral hydrogen fraction. The relative measurement is attempted here for ULAS J1319+0950, once again following the methodology of Fan et al. (2006a), by defining the quasar proximity region as the volume within which the transmitted flux fraction is $\lesssim 0.1$. After dividing the Gemini spectrum by the continuum+line fit (described in Section 4.2) to convert to transmitted flux, the spectrum was smoothed to a resolution of 20 Å. This smoothed transmission spectrum remains below 0.1 down to a wavelength of $\lambda \approx 0.856 \mu\text{m}$; converting to redshift and then to a co-moving physical length implies that ULAS J1319+0950 has a proximity zone of radius $R_p \approx 5.1 \text{ Mpc}$.

The inferred radius is broadly consistent with measurements from optically-detected SDSS quasars (Fan et al. 2006a), although to make a more quantitative comparison it is necessary to standardise the above measurement of R_p to a fiducial absolute magnitude $M_{1450,\text{AB}} = -27$ according to $R_{p,27} = 10^{0.4(M_{1450,\text{AB}}+27)} R_p$. With $M_{1450,\text{AB}} = -27.12$ this gives $R_{p,27} \approx 4.9 \text{ Mpc}$ for ULAS J1319+0950. This is lower than the fiducial value of $\sim 7 \text{ Mpc}$ given by Fan et al. (2006a) for $z \approx 6.1$ quasars, although this difference is not significant given the range of $R_{p,27}$ values seen in the optical sample.

5. ULAS J0203+0012

ULAS J0203+0012 was the first $z \approx 6$ quasar found in UKIDSS, Venemans et al. (2007) describing the discovery and reporting a redshift of $z = 5.86$. The source was subsequently recovered by Jiang et al. (2008) in their survey for high-redshift quasars using deep co-added data from multiple scans of SDSS Stripe

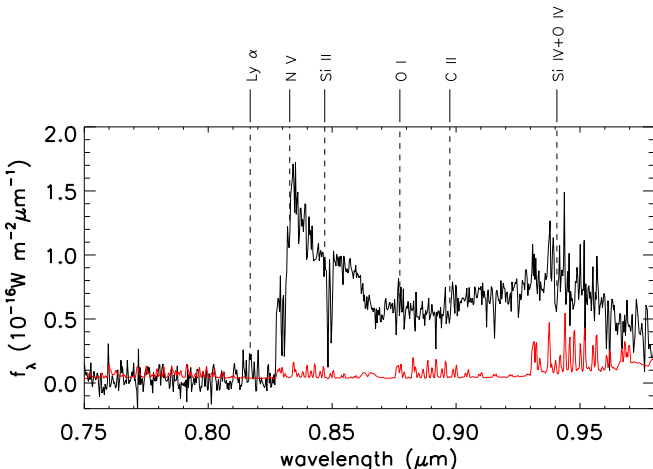


Fig. 6. Re-calibrated VLT spectrum of ULAS J0203+0012 (black curve) and the noise spectrum (red curve), binned by a factor of two. The wavelengths of common emission lines redshifted by $z = 5.72$ are indicated.

82; they quote a redshift of $z = 5.85$. An improved redshift for ULAS J0203+0012 was sought by acquiring a NIR spectrum (Section 5.1). These data revealed ULAS J0203+0012 to be a broad-absorption line (BAL) quasar, resulting in a modified redshift estimate (Section 5.2), and also showing some discrepancies compared to the existing optical spectrum in the region $0.9\text{--}1.0\,\mu\text{m}$. The origin of the discrepancy was traced to the relatively poor quality of the published standard star data used to flux-calibrate the optical spectrum, which has hence been re-reduced (Section 5.1).

5.1. Spectroscopic observations

5.1.1. Optical spectrum

The original optical spectroscopic observations of ULAS J0203+0012 were made in 2006 September using the FOcal Reducer and low dispersion Spectrograph (FORS2) on the Very Large Telescope (VLT), and are described in detail in Venemans et al. (2007). The re-reduction followed a similar sequence to that described there, up to the point of flux calibration. Instead of using the published spectrophotometry of the white dwarf standard star GD50 from Oke (1990), a model spectrum with effective temperature $T_{\text{eff}} = 41150\,\text{K}$ and surface gravity $\log[g/(1\,\text{cm}\,\text{s}^{-2})] = 9.15$ from Dobbie et al. (2005) was used to establish the flux calibration curve. Finally, the data were scaled to match the measured z -band photometry. The revised spectrum, plotted in Fig. 6, shows a sharp downturn longward of $0.95\,\mu\text{m}$ compared to the original spectrum.

5.1.2. NIR spectrum

A NIR spectrum of ULAS J0203+0012 was obtained using the Gemini Near Infra-Red Spectrograph (GNIRS) on the Gemini South Telescope on the night beginning 2007 March 22. The observations were taken in cross-dispersed mode with the short camera, the 32 lines mm^{-1} grism, and a $0''.75$ slit, providing coverage from $\sim 0.8\,\mu\text{m}$ to $\sim 2.5\,\mu\text{m}$ at a resolving power of $R = 500$. Due to the limited slit length it was impractical to adopt the observation strategy used for the NIRI observations of ULAS J1319+0950 (Section 4.1) and so a standard ABBA offset pattern was used.

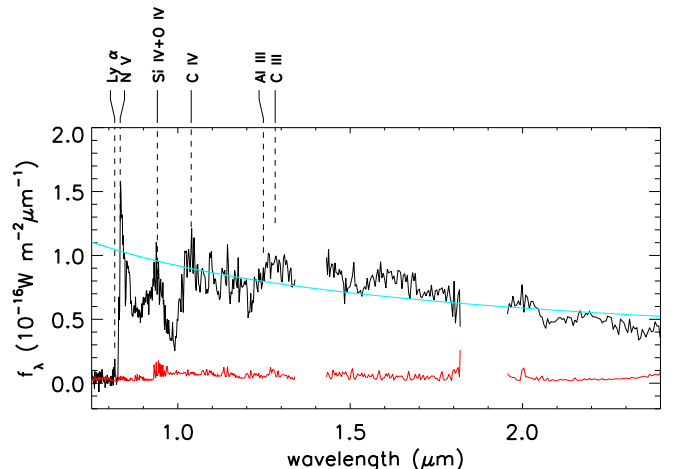


Fig. 7. The combined optical and NIR spectrum, spliced at $\lambda = 0.96\,\mu\text{m}$, of ULAS J0203+0012 (black curve) and the noise spectrum (red curve), both binned by a factor of eight. The power-law continuum fit is also shown (blue). The wavelengths of common emission lines redshifted by $z = 5.72$ are indicated. The Mg II line would be expected to appear at $1.88\,\mu\text{m}$, in the middle of the strong telluric absorption band at $\sim 1.9\,\mu\text{m}$ for which the data have been omitted.

The observations comprise eight frames, with a total exposure time of 2400 s. The data were reduced mainly using the Gemini-GNIRS package in the Image Reduction and Analysis Facility (IRAF; Tody 1993). After correction for pattern noise and flat-fielding, each of the diffraction orders was separated, and the double-subtraction method (described in Section 4.1) was applied to each of the four pairs of images. The resulting four frames for each order were then averaged. S-distortion correction and wavelength calibration were then applied using observations of an Ar lamp, and one-dimensional spectra were extracted. The data were corrected for telluric absorption and flux-calibrated using the spectrum of a spectroscopic standard star. Finally, the different diffraction orders were spliced together to produce a single continuous spectrum. Strong telluric absorption bands occur at $1.35\text{--}1.43\,\mu\text{m}$ and $1.80\text{--}1.95\,\mu\text{m}$, and so the data in these wavelength ranges were discarded. The spectrum was placed on an absolute flux scale by matching to the K -band photometry.

Comparison of the optical and NIR spectra in the region of overlap ($0.8\text{--}1.0\,\mu\text{m}$) showed good detailed agreement, except for a 10 per cent normalisation offset, and so the optical spectrum was scaled to the NIR spectrum. The declining S/N of the NIR spectrum towards the blue, and of the optical spectrum towards the red, are approximately equal at $0.96\,\mu\text{m}$, so the two spectra were spliced at this point. The final combined spectrum is plotted in Fig. 7.

5.2. Redshift estimation

The most striking features of the combined ULAS J0203+0012 spectrum shown in Fig. 7 are the broad absorption lines near $0.9\,\mu\text{m}$ and $1.0\,\mu\text{m}$. These are attributed to Si IV and C IV, respectively. Despite the increased wavelength coverage, the redshift is difficult to determine accurately, as is common with BAL quasars (e.g. Trump et al. 2006). Venemans et al. (2007) and Jiang et al. (2008) identified the peak of the line near $0.835\,\mu\text{m}$ with Ly α , and the shoulder at $0.855\,\mu\text{m}$ with N V, but matching Si IV, C IV and C III lines for this redshift are not evident. Instead

it seems likely that the peak at $0.835\text{ }\mu\text{m}$ is the N v emission line, and that the Ly α emission line has been absorbed by a N v BAL. As shown in Fig. 7, a redshift of $z = 5.72$ provides a reasonable match to the N v peak, as well as weak features that match Si iv, C iv, and C m]; but any redshift in the range $5.70 < z < 5.74$ is consistent with the data. Unfortunately the Mg ii line, which ought to give a definitive redshift, lies in the region of atmospheric absorption near $1.9\text{ }\mu\text{m}$.

In the wavelength region $0.85\text{--}1.08\text{ }\mu\text{m}$ it is difficult to determine the extent of the BAL troughs, and the regions of unabsorbed continuum emission. The best fit power-law, plotted in Fig. 7, is a poor match. It seems likely that the sharp step near $0.865\text{ }\mu\text{m}$ marks the blue edge of the Si iv BAL, and that the shoulder at $0.855\text{ }\mu\text{m}$, previously identified with N v, is in fact continuum emission. The resulting estimate of the rest frame equivalent width of the N v line is $\sim 4.2\text{ \AA}$.

Given the presence of BAL troughs, it is difficult to infer very much about the neutral hydrogen along the line-of-sight to ULAS J0203+0012, as the Ly α emission line is all but completely absorbed. Similarly, it is not possible to measure the Gunn & Peterson (1965) optical depth to ULAS J0203+0012: assuming the N v BAL has a similar velocity width to the C iv and Si iv BALs, the absorption blueward of Ly α is most likely dominated by the wing of the N v BAL, and not by intervening neutral hydrogen along the line-of-sight.

The case of ULAS J0203+0012 is rather similar to that of the BAL quasar SDSS J1044–0125 (Fan et al. 2000). The initial redshift measurement of $z = 5.80$ by Fan et al. (2000) was revised to $z = 5.74$ by Goodrich et al. (2001) on the basis of NIR spectroscopy, after which Jiang et al. (2007) used the C m] line to estimate $z = 5.78$. Both ULAS J0203+0012 and SDSS J1044–0125 demonstrate the importance of NIR spectra to obtaining reliable redshifts of $z \approx 6$ quasars (and especially BALs).

6. Conclusions and future prospects

Two new high-redshift quasars have now been discovered in the UKIDSS LAS: ULAS J0203+0012 at $z = 5.72$ (previously given as $z = 5.86$; Venemans et al. 2007); and ULAS J1319+0950 at $z = 6.13$. Two previously known high-redshift quasars, SDSS 0836+0054 at $z = 5.82$ (Fan et al. 2001) and SDSS 1411+1217 at $z = 5.93$ (Fan et al. 2004), have also been recovered in the UKIDSS DR3 LAS area. The two new quasars are well within the redshift range covered by optical surveys, but they were both too faint in SDSS to be included in the high-redshift quasar sample defined by Fan et al. (2003). While the revised lower redshift of ULAS J0203+0012 puts its Ly α emission near the peak of the SDSS z band response, the line is almost completely absorbed by a N v BAL, which results in a reduction of the z -band flux. ULAS J1319+0950 has a very weak Ly α line, with a rest-frame equivalent width of just $\sim 20\text{ \AA}$. The small Ly α equivalent width results in the z -band S/N falling marginally below the limit of the SDSS quasar sample defined by Fan et al. (2003). Nonetheless, the detection of four $z \approx 6$ quasars brighter than $Y_{\text{Vega}} = 19.88$ in the 870 deg^2 of UKIDSS DR3 LAS is consistent with expectations from the luminosity function of Jiang et al. (2008), and so these new detections do not imply the existence of a previously unidentified quasar population with weak emission features.

These results demonstrate that the UKIDSS data are of sufficient quality to recover $z \gtrsim 6$ quasars down to $Y \approx 19.5$ with reasonable completeness. Quantification of the completeness will

be explored in more detail when the sample is larger. At the time of writing the UKIDSS Fifth Data Release (DR5; Warren et al. 2009) has already taken place, increasing the LAS area covered in the Y and J bands to $\sim 1360\text{ deg}^2$. DR5 is of sufficient size that finding no quasars of redshift $z > 6.4$ would be somewhat inconsistent with expectations.

Acknowledgements. Many thanks to the staffs of UKIRT, the Cambridge Astronomical Survey Unit, and the Wide Field Astronomy Unit, Edinburgh, for their work in implementing UKIDSS. Thanks to Marie Lemoine-Busserolle, Kathy Roth and Claudia Winge for help in setting up the Gemini observations. Paul Dobbie kindly provided the synthetic spectrum of GD50 used for flux-calibrating the optical spectrum of ULAS J0203+0012.

Based on observations obtained at the Gemini Observatory (acquired through the Gemini Science Archive), which is operated by the Association of Universities for Research in Astronomy, Inc., under a cooperative agreement with the NSF on behalf of the Gemini partnership: the National Science Foundation (United States), the Science and Technology Facilities Council (United Kingdom), the National Research Council (Canada), CONICYT (Chile), the Australian Research Council (Australia), CNPq (Brazil) and SECYT (Argentina).

The Liverpool Telescope is operated on the island of La Palma by Liverpool John Moores University in the Spanish Observatorio del Roque de los Muchachos of the Instituto de Astrofísica de Canarias with financial support from the UK Science and Technology Facilities Council.

MP acknowledges support from the University of London's Perren Fund. PCH, RGM and BV acknowledge support from the STFC-funded Galaxy Formation and Evolution programme at the Institute of Astronomy.

The referee, Michael Strauss, made a number of valuable suggestions which have significantly improved this paper.

References

- Adelman-McCarthy, J. K. et al. 2007, ApJS, 172, 634
- Barkana, R. & Loeb, A. 2001, Phys. Rep., 349, 125
- Becker, R. H., Fan, X., White, R. L., & et al. 2001, AJ, 122, 2850
- Bennett, C. L., Bay, M., Halpern, M., et al. 2003, ApJ, 583, 1
- Casali, M., Adamson, A., Alves de Oliveira, C., et al. 2007, A&A, 467, 777
- Diamond-Stanic, A. M., Fan, X., Brandt, W. N., et al. 2009, ApJ, 699, 782
- Dobbie, P. D., Burleigh, M. R., Levan, A. J., et al. 2005, MNRAS, 357, 1049
- Dunkley, J., Komatsu, E., Nolta, M. R., et al. 2009, ApJS, 180, 306
- Dye, S., Warren, S. J., Hambly, N. C., et al. 2006, MNRAS, 372, 1227
- Emerson, J. P., Sutherland, W. J., McPherson, A. M., et al. 2004, The Messenger, 117, 27
- Fan, X., Hennawi, J. F., Richards, G. T., & et al. 2004, AJ, 128, 515
- Fan, X., Narayanan, V. K., Lupton, R. H., & et al. 2001, AJ, 122, 2833
- Fan, X., Narayanan, V. K., Strauss, M. A., et al. 2002, AJ, 123, 1247
- Fan, X., Strauss, M. A., Becker, R. H., et al. 2006a, AJ, 132, 117
- Fan, X., Strauss, M. A., Gunn, J. E., et al. 1999, ApJ, 526, L57
- Fan, X., Strauss, M. A., Richards, G. T., & et al. 2006b, AJ, 131, 1203
- Fan, X., Strauss, M. A., Schneider, D. P., & et al. 2003, AJ, 125, 1649
- Fan, X., White, R. L., Davis, M., et al. 2000, AJ, 120, 1167
- Glikman, E., Eigenbrod, A., Djorgovski, S. G., et al. 2008, AJ, 136, 954
- Goodrich, R. W., Campbell, R., Chaffee, F. H., et al. 2001, ApJ, 561, L23
- Gunn, J. E. & Peterson, B. A. 1965, ApJ, 142, 1633
- Haislip, J. B., Nysewander, M. C., Reichart, D. E., et al. 2006, Nature, 440, 181
- Hambly, N. C., Collins, R. S., Cross, N. J. G., et al. 2008, MNRAS, 384, 637
- Hazard, C., Mackey, M. B., & Shimmins, A. J. 1963, Nature, 197, 1037
- Hewett, P. C., Warren, S. J., Leggett, S. K., & Hodgkin, S. T. 2006, MNRAS, 367, 454
- Irwin, M. J., Lewis, J., Hodgkin, S. T., & Gonzales-Solares. 2009, MNRAS, in preparation
- Iye, M., Ota, K., Kashikawa, N., et al. 2006, Nature, 443, 186
- Jiang, L., Fan, X., Annis, J., et al. 2008, AJ, 135, 1057
- Jiang, L., Fan, X., Vestergaard, M., et al. 2007, AJ, 134, 1150
- Kurk, J. D., Walter, F., Fan, X., et al. 2007, ApJ, 669, 32
- Lawrence, A., Warren, S. J., Almaini, O., et al. 2007, MNRAS, 379, 1599
- Mortlock, D. J., Patel, M., Warren, S. J., et al. 2009, MNRAS, submitted
- Oke, J. B. 1990, AJ, 99, 1621
- Rousselot, P., Lidman, C., Cuby, J.-G., Moreels, G., & Monnet, G. 2000, A&A, 354, 1134
- Schmidt, M. 1963, Nature, 197, 1040
- Schneider, D. P. 1999, in American Institute of Physics Conference Series, Vol. 470, After the Dark Ages: When Galaxies were Young (the Universe at $2 < z < 5$), ed. S. Holt & E. Smith, 233
- Skrutskie, M. F., Cutri, R. M., Stiening, R., et al. 2006, AJ, 131, 1163

- Strömgren, B. 1939, ApJ, 89, 526
Tody, D. 1993, in Astronomical Society of the Pacific Conference Series, Vol. 52,
Astronomical Data Analysis Software and Systems II, ed. R. J. Hanisch,
R. J. V. Brissenden, & J. Barnes, 173
Trump, J. R., Hall, P. B., Reichard, T. A., et al. 2006, ApJS, 165, 1
Tytler, D. & Fan, X.-M. 1992, ApJS, 79, 1
van Dokkum, P. G. 2001, PASP, 113, 1420
Venemans, B. P., McMahon, R. G., Warren, S. J., et al. 2007, MNRAS, 376, L76
Walter, F., Carilli, C., Bertoldi, F., et al. 2004, ApJ, 615, L17
Warren, S. J., Hambly, N. C., Dye, S., et al. 2007, MNRAS, 375, 213
Warren, S. J., Hambly, N. C., Lawrence, A., et al. 2009, MNRAS, in preparation
Weatherley, S. J., Warren, S. J., Møller, P., et al. 2005, MNRAS, 358, 985
Willott, C. J., Delorme, P., Omont, A., et al. 2007, AJ, 134, 2435
Wyithe, J. S. B., Warszawski, L., Geil, P. M., & Oh, S. P. 2009, MNRAS, 395,
311
York, D. G. et al. 2000, AJ, 120, 1579